Continental Geometry's Role in Shaping Wintertime Temperature Variance

NICOLE K. NEUMANN[a] AND NICHOLAS J. LUTSKO[b]

[a] *Lamont-Doherty Earth Observatory, Columbia University, Palisades, New York*
[b] *Scripps Institution of Oceanography, University of California, San Diego, La Jolla, California*

(Manuscript received 1 December 2021, in final form 4 August 2022)

ABSTRACT: The factors controlling the present-day pattern of temperature variance are poorly understood. In particular, it is unclear why the variance of wintertime near-surface temperatures on daily and synoptic time scales is roughly twice as high over North America as over Eurasia. In this study, continental geometry's role in shaping regional wintertime temperature variance is investigated using idealized climate model simulations run with midlatitude continents of different shapes. An isolated, rectangular midlatitude continent suggests that in the absence of other geographic features, the highest temperature variance will be located in the northwest of the continent, roughly collocated with the region of largest meridional temperature gradients, and just north of the maximum near-surface wind speeds. Simulations with other geometries, mimicking key features of North America and Eurasia, investigate the impacts of continental length and width, sloping coastlines, and inland bodies of water on regional temperature variance. The largest effect comes from tapering the northwest corner of the continent, similar to Eurasia, which substantially reduces the maximum temperature variance. Narrower continents have smaller temperature variance in isolation, implying that the high variances over North America must be due to the nonlocal influence of stationary waves. Support for this hypothesis is provided by simulations with two midlatitude continents, which show how continental geometry and stationary waves can combine to shape regional temperature variance.

SIGNIFICANCE STATEMENT: Wintertime temperature variance over North America is roughly twice as high as over Eurasia, but the reasons for this are unknown. Here we use idealized climate model simulations to investigate how continental geometry shapes regional temperature variance. We find that the smaller variance over Eurasia is largely due to the tapering of its northwest coast, which weakens temperature gradients in the continental interior. Our simulations also suggest that in isolation a narrow continent, like North America, should have weak temperature variance, implying that stationary waves are responsible for the high variance over North America. Understanding the controls on regional temperature variance is important for interpreting present-day winter climates and how these will change in the future.

KEYWORDS: Atmospheric circulation; Atmosphere-land interaction; Regional effects; Surface temperature; Subseasonal variability

1. Introduction

In winter, the weather over North America is much more variable than the weather over Eurasia: depending on the precise regions that are averaged over, the variance of wintertime near-surface temperatures on daily and synoptic time scales is roughly twice as high over North America as it is over Eurasia (Fig. 1, Table 1). So, while the coldest temperatures in the Northern Hemisphere tend to be found in northern Siberia, central Canada and the Great Plains region just east of the Rockies experience the largest daily and weekly temperature swings of anywhere on Earth.

The factors responsible for the difference in temperature variance between the two continents are poorly understood. Several recent studies have investigated what controls the variance and higher-order moments of temperature distributions in zonally symmetric climates (e.g., Schneider et al. 2015; Garfinkel and Harnik 2017; Holmes et al. 2016; Linz et al. 2018, 2020), motivated in part by the growing recognition that changes in temperature variance and temperature extremes in future warm climates may be just as impactful as changes in mean temperature. Another area of focus has been the impacts of the Arctic Amplification of warming and of Arctic sea ice loss on midlatitude weather (Cohen et al. 2014; Screen 2014; Schneider et al. 2015; Hoskins and Woollings 2015; Barnes and Polvani 2015; Screen et al. 2018; Screen and Blackport 2019; Blackport et al. 2019), while Tamarin-Brodsky et al. (2019, 2020) examined the relationships between regional warming patterns and changes in temperature distributions more generally. Recently, Zhang et al. (2022) used the conditional mean framework of Linz et al. (2020) to quantify the relative contribution of horizontal temperature advection, as opposed to other physical processes such as diabatic heating and radiation, to the shapes of daily temperature distributions in reanalysis data. But none of these studies have addressed the dynamical mechanisms that cause the temperature variance in one region to differ from the variance in another region at the same latitude.

In winter, daily and synoptic temperature variability at midlatitudes are largely determined by horizontal advection (Zhang et al. 2022), in contrast to summer when other processes, such as convection and land–atmosphere interactions,

Denotes content that is immediately available upon publication as open access.

Corresponding author: Nicholas Lutsko, nlutsko@ucsd.edu

DOI: 10.1175/JCLI-D-21-0925.1

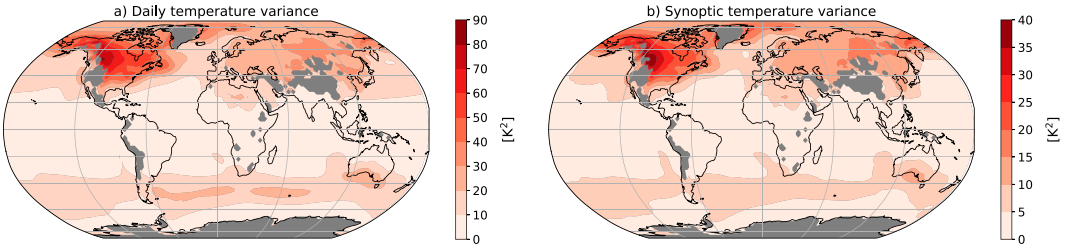

FIG. 1. (a) Variance of December–February (DJF) 850-hPa daily temperatures for the period 1979–2020, calculated using data taken from the ERA5 dataset. Locations where topography intrudes through 850 hPa are masked in gray. (b) As in (a), but data are filtered using a fourth-order Butterworth filter to only retain power at synoptic time scales, defined here as 3–15 days.

also contribute to synoptic variability (e.g., Fischer and Schär 2009; Vargas Zeppetello and Battisti 2020). The importance of horizontal advection has led to the suggestion that wintertime temperature variability is closely related to mean horizontal temperature gradients, particularly meridional temperature gradients, so that

$$\overline{T'^2} \approx L_y^2\left(\frac{\partial \overline{T}}{\partial y}\right)^2 + L_x^2\left(\frac{\partial \overline{T}}{\partial x}\right)^2 + L_x L_y \frac{\partial \overline{T}}{\partial x}\frac{\partial \overline{T}}{\partial y} \approx L_y^2\left(\frac{\partial \overline{T}}{\partial y}\right)^2, \quad (1)$$

where T is temperature, L_y is a characteristic mixing length in the meridional (y) direction, L_x is a characteristic mixing length in the zonal (x) direction, the overbars denote averages over appropriate spatial and temporal scales, and primes denote departures from these averages (note that we use Cartesian coordinates for simplicity, but all variables should be taken to be on the sphere). The second approximate equality assumes that meridional temperature gradients are much larger than zonal temperature gradients, which is generally true for Earth's climate. The assumptions underlying Eq. (1) are discussed further in section 2b, below. The large variance of wintertime temperatures over North America is associated with both strong meridional temperature gradients (Lutsko et al. 2019) and high meridional wind variances (i.e., large effective mixing lengths; see Simpson et al. 2020), but what causes these high values is still unclear.

The link between temperature variance and temperature gradients suggests that the Northern Hemisphere winter stationary wave field plays an important role in setting the pattern of regional temperature variance (note that by enhancing the generation of baroclinic eddies, large temperature gradients also lead to high eddy kinetic energy and by extension, high wind variance). But stationary waves only determine the near-surface response to wave sources, such as topography and diabatic heating, sufficiently downstream of the sources for the external Rossby mode to emerge from the continuum of waves that are excited (Held et al. 1985). Closer to the source, the response is more complicated. Thus, while understanding what sets the boreal winter stationary wave pattern is an important step toward explaining the pattern of wintertime temperature variance (see, e.g., Held et al. 2002; Garfinkel et al. 2020), the two questions are not equivalent.

One important factor governing Northern Hemisphere temperature distributions is orography. Theoretical arguments and

TABLE 1. List of model experiments, maximum winter daily 850-hPa temperature variance, and reanalysis values.

Expt name	Description	Max temperature variance (K^2)
Control	Covers 30°–70°N, 100°–235°E	83
Narrow	Covers 30°–70°N, 100°–160°E	61
Long	Covers 0°–70°N, 100°–235°E	78
Slanted	As in Control, but southeast corner at 30°N, 220°E and northeast corner at 70°N, 250°E,	70
Tapered	As in Control, but northwest corner at 45°N, 100°E and additional corner at 70°N, 160°E	65
GOM	As in Control, but gulf inland to 40°N, 150°E and 40°N, 180°E	88
Inland Sea	As in Control, but inland sea with corners at 35°N, 130°E;45°N, 130°E; 35°N, 160°E; and 45°N, 160°E	78
2 Continents (wide and narrow)	Wide covers 30°–70°N, 0°–120°E	69
	Narrow covers 30°–70°N, 220°–300°E	77
2 Continents + Tapering (wide and narrow)	Wide is as in 2 Continents, but has corners at 45°N, 0°E and 70°N, 60°E	61
	Narrow is as in 2 Continents	65
ERA5 (Eurasia and North America)	Eurasia	44
	North America	86

idealized climate model simulations suggest that temperature variance should be enhanced immediately downstream and reduced immediately upstream of mountain ranges (Lutsko et al. 2019). Hence, the Rockies, on the west coast of North America, enhance North American temperature variance, while the Tibetan Plateau, the Himalayas, and the Mongolian Mountains, on the east coast of Eurasia, damp Eurasian temperature variance. However, comprehensive climate model simulations in which these mountain ranges were flattened demonstrated that orography only explains about 25% of the difference in temperature variance between the two continents (Lutsko et al. 2019), leaving the majority still unexplained.

Eurasia and North America have many other distinctive geographic features which could affect their near-surface temperature variance. Eurasia is much wider than North America, so warm ocean air does not penetrate as far into the continental interior (McKinnon et al. 2013). As another example, the east coast of North America slopes northeast–southwest, which affects the North Atlantic storm track (Brayshaw et al. 2009) and could influence temperature variability along the North American east coast. These features, and others, may be important for regional temperature variance, but so far their effects have not been systematically investigated.

In this study, we take a step toward a better understanding of regional temperature variance by examining the role of continental geometry. We do this using simulations with an idealized general circulation model (GCM) designed to mimic the key geographic features of North America and Eurasia (see section 2a for descriptions of the model and experiments). The model uses a slab ocean and "land" is represented by reduced mixed-layer depths, allowing us to focus on the role of land–ocean differences in heat capacity. We leave the additional complexity of land surface processes for future work.

We begin the presentation of our results by describing the winter climate of a generic, rectangular midlatitude continent (section 3). To our knowledge, this case has not been described before, and it represents a kind of "null hypothesis" for continental temperature distributions at midlatitudes in the absence of notable geographic features. Next, we examine temperature variability in a set of simulations that mimic key features of Eurasia and North America (section 4), before exploring how the results change in a hemisphere with two continents, instead of a single isolated continent (section 5). Regional differences in mixing lengths are not thought to be a key part of regional differences in temperature variance, but in section 6 we discuss factors setting the effective mixing lengths in the simulations. We end with conclusions in section 7.

2. Methods

a. Idealized climate model and experiments

The GCM numerically solves the primitive equations on the sphere and is forced by a gray radiation scheme (Frierson et al. 2006). The GCM is coupled to a slab ocean, with no representation of ocean dynamics or sea ice, and the model uses the simplified Betts–Miller (SBM) convection scheme of Frierson (2007). All experiments were conducted using a convective relaxation time scale τ_{SBM} of 2 h and a reference relative humidity $\mathrm{RH}_{\mathrm{SBM}} = 0.7$, and the boundary layer scheme is the one used by O'Gorman and Schneider (2008).

The GCM was integrated at T85 truncation (corresponding to a resolution of roughly 1.4° × 1.4° on a Gaussian grid) with 40 vertical levels, starting from a state with uniform SSTs. A mixed-layer depth of 20 m was used to represent ocean surfaces, and a reduced depth of 0.05 m was used to represent "land." All simulations were performed with a full seasonal cycle of insolation, and were conducted for 16 years, with the first year discarded as spinup. The interannual variability of temperature variance is large in these simulations (10%–20% of the climatological variance), and we have run some simulations for longer to ensure the qualitative robustness of our findings.

"Winter" is defined as the 90 days during which the Northern Hemisphere receives the least insolation, and we present results from nine simulations, shown in Fig. 2 and listed in Table 1.

b. Stationary eddy temperature and temperature variance budgets

To help interpret the simulations, we will analyze the stationary eddy temperature and temperature variance budgets at 850 hPa. The steady-state stationary eddy temperature budget at a given atmospheric level can be written as

$$(\overline{\mathbf{v}} \cdot \boldsymbol{\nabla}\overline{T})^* + \left(\overline{\omega}\frac{\partial \overline{T}}{\partial p}\right)^* + \boldsymbol{\nabla} \cdot (\overline{\mathbf{v}'T'})^* + \left(\overline{\omega'\frac{\partial T'}{\partial p}}\right)^* = F(\overline{T}^*) - D(\overline{T}^*), \tag{2}$$

where $\mathbf{v}$ is the near-surface horizontal wind vector; ω is the vertical pressure velocity; $\boldsymbol{\nabla}$ is the two-dimensional gradient or divergence in x and y; p is pressure; $F(\overline{T}^*)$ and $D(\overline{T}^*)$ are sources and sinks of eddy temperatures, respectively; the asterisks denote a zonal anomaly; the overbars now denote time averages; and the primes are now deviations from the time averages. In winter climates, the first term on the left-hand side is the most important advective term, and can be decomposed into three components:

$$(\overline{\mathbf{v}} \cdot \boldsymbol{\nabla}\overline{T})^* = \underbrace{[\overline{\mathbf{v}}] \cdot \boldsymbol{\nabla}\overline{T}^*}_{\text{mean flow advection}} + \underbrace{\overline{\mathbf{v}}^* \cdot \boldsymbol{\nabla}[\overline{T}]}_{\text{eddy advection}} + \underbrace{\overline{\mathbf{v}}^* \cdot \boldsymbol{\nabla}\overline{T}^*}_{\text{nonlinear eddy advection}}, \tag{3}$$

where square brackets denote zonal averages.

The steady-state temperature variance budget at a given level is obtained by taking the budget for temporal temperature anomalies (T'), multiplying by T', and time averaging:

$$\overline{\overline{\mathbf{v}} \cdot \boldsymbol{\nabla}(T'^2/2)} + \overline{\mathbf{v}'T'} \cdot \boldsymbol{\nabla}\overline{T} + \overline{\mathbf{v}' \cdot \boldsymbol{\nabla}(T'^2/2)} \approx F(T'^2) - D(T'^2), \tag{4}$$

where $F(T'^2)$ and $D(T'^2)$ are sources and sinks of temperature variance, respectively. We assume that in winter near-surface temperature variance is primarily generated by horizontal advection, so that the vertical terms can be ignored (i.e., convection is negligible).

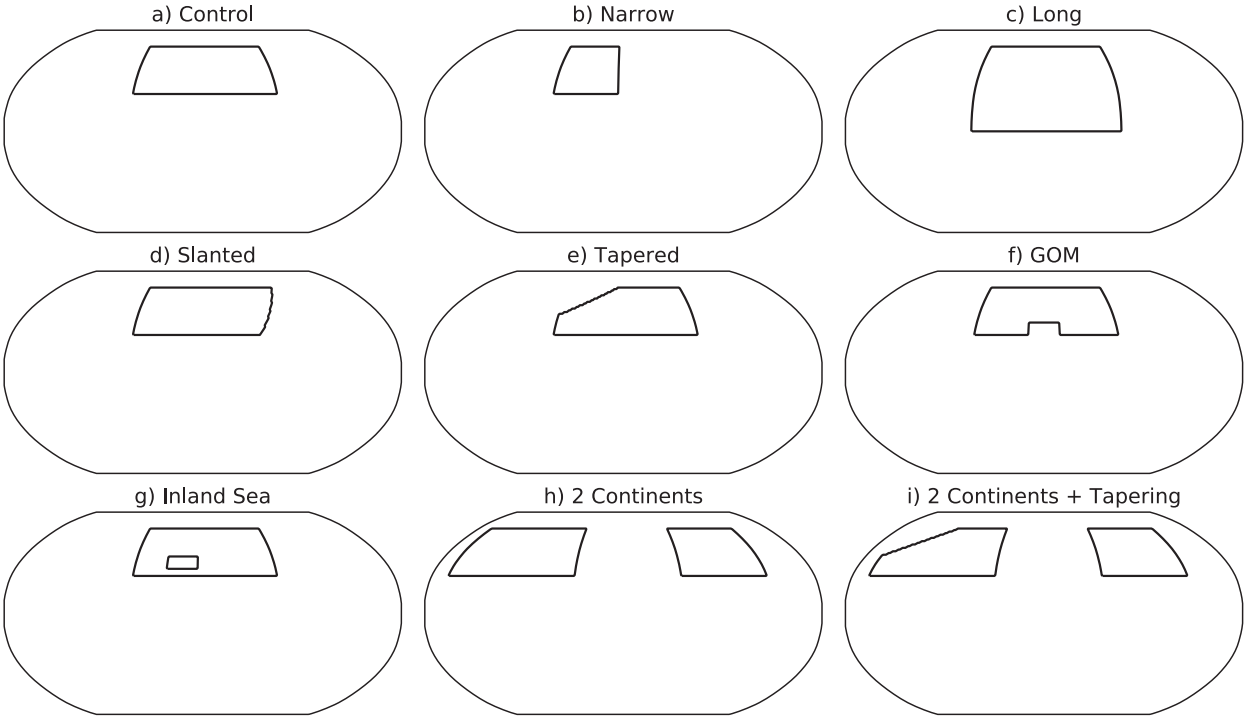

FIG. 2. Land geometries used in the nine simulations with the moist GCM. See Table 1 for details of each configuration.

Equation (1) in the introduction is obtained from a Taylor expansion of T' (Schneider et al. 2015), but it can also be derived directly from the temperature variance budget. Implicitly, Eq. (1) assumes that the second term on the left hand side ($\overline{\mathbf{v}'T'} \cdot \boldsymbol{\nabla}\overline{T}$) dominates the variance budget, with the mean flow term $[\overline{\mathbf{v}} \cdot \boldsymbol{\nabla}(\overline{T'^2}/2)]$ and the nonlinear term $[\mathbf{v}' \cdot \boldsymbol{\nabla}(\overline{T'^2}/2)]$ assumed small. As shown by Linz et al. (2020) and Zhang et al. (2022), the non-advective terms of temperature variance can be approximated as relaxation to an equilibrium temperature field:

$$\overline{\overline{\mathbf{v}} \cdot \boldsymbol{\nabla}(\overline{T'^2}/2)} + \overline{\mathbf{v}'T'} \cdot \boldsymbol{\nabla}\overline{T} + \overline{\mathbf{v}' \cdot \boldsymbol{\nabla}(\overline{T'^2}/2)} \approx -\frac{\overline{T'^2}}{\tau_{\mathrm{eq}}}, \tag{5}$$

where τ_{eq} is a restoration time scale. If transient eddy heat transport is taken to be diffusive (Kushner and Held 1998), then

$$\overline{\mathbf{v}'T'} \approx -D\boldsymbol{\nabla}\overline{T} = -\frac{L^2}{\tau_m}\boldsymbol{\nabla}\overline{T},$$

where L is a characteristic mixing length and τ_m is a characteristic mixing time scale. Hence,

$$\overline{\mathbf{v}'T'} \cdot \boldsymbol{\nabla}\overline{T} \approx -\frac{L^2}{\tau_m}(\boldsymbol{\nabla}\overline{T})^2,$$

and for a steady state the temperature variance budget can be approximated as

$$\frac{L^2}{\tau_m}(\boldsymbol{\nabla}\overline{T})^2 \approx \frac{\overline{T'^2}}{\tau_{\mathrm{eq}}}$$

or

$$\overline{T'^2} \approx \frac{\tau_{\mathrm{eq}}}{\tau_m}L^2(\boldsymbol{\nabla}\overline{T})^2, \tag{6}$$

which is similar to Eq. (1), but introduces two time scales: τ_{eq}, the time scale on which local temperature anomalies are restored by radiation and other processes, and the diffusive τ_m. We emphasize again that the assumptions which lead to Eq. (6) are most applicable to the winter midlatitudes, and this equation is less relevant to other regions and seasons.

As shown by Caballero and Hanley (2012), the lower tropospheric eddies which transport moisture (and heat) are almost stationary with respect to the background flow, so τ_m can be taken to be a linear eddy damping coefficient, like friction (see also Ferrari and Nikurashin 2010). Mixing lengths can then be written in terms of τ_m and the eddy kinetic energy (EKE) as $L = \tau_m\sqrt{\mathrm{EKE}}$, which makes the connection between friction and temperature variance clearer:

$$\overline{T'^2} \approx \tau_{\mathrm{eq}}\tau_m \mathrm{EKE}(\boldsymbol{\nabla}\overline{T})^2. \tag{7}$$

Equation (7) can be used to explain why temperature variance is typically higher over land than over oceans: the thermal inertia of the ocean means that turbulent surface energy fluxes quickly damp atmospheric temperature fluctuations, whereas over land the surface quickly equilibrates to the atmospheric temperature, so the equilibration time scale is primarily determined by radiative processes rather than faster acting turbulent processes. This implies a larger τ_{eq} value over

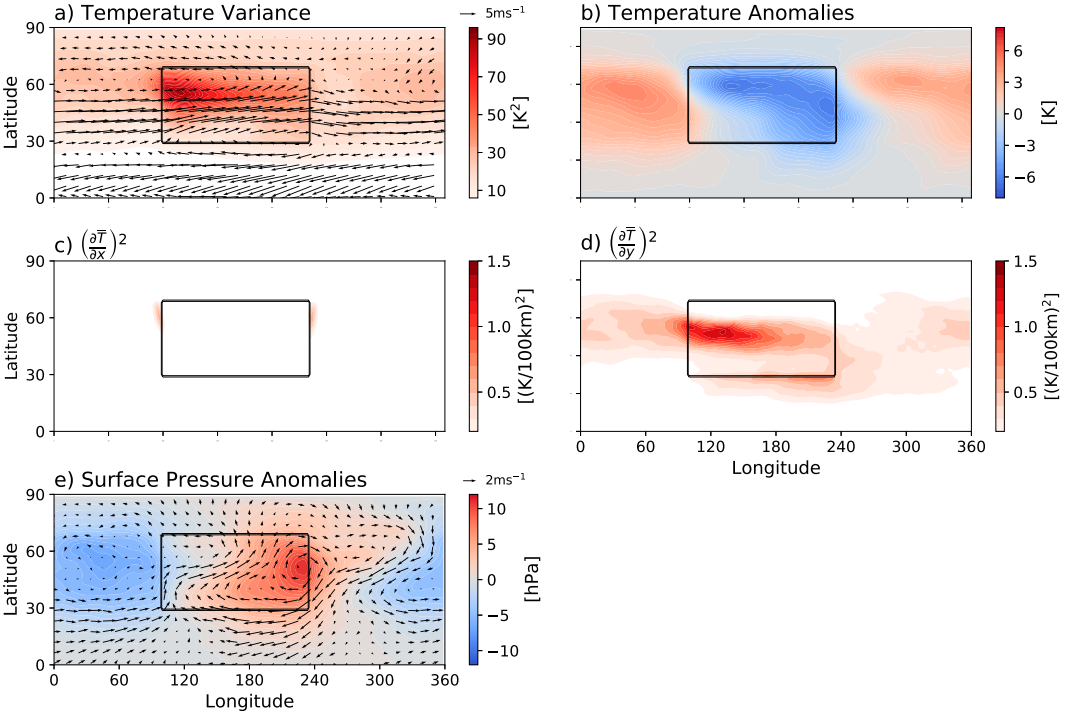

FIG. 3. (a) Variance of wintertime 850-hPa daily temperature in the Control simulation (colored contours) and 850-hPa winds (arrows). (b) Mean wintertime zonal 850-hPa temperature anomalies in the same simulation. (c) Mean wintertime squared zonal 850-hPa temperature gradients in the same simulation. (d) Mean wintertime squared meridional 850-hPa temperature gradients in the same simulation. (e) Mean wintertime zonal surface pressure (colored contours) and 850-hPa zonal wind anomalies (arrows) in the same simulation.

land than over ocean and, via Eq. (7), higher temperature variance there. By not accounting for the two relevant time scales, Eq. (1) cannot explain the larger temperature variances over land.

3. Winter climate of an isolated midlatitude continent

The Control simulation consists of an isolated, rectangular midlatitude continent (Fig. 2a). The highest daily near-surface (850 hPa) winter temperature variance is located in the northwest of the continent (Fig. 3a), with a maximum value of 84 K^2, and the variance decreases moving to the east and to the south, with the weakest temperature variance found along the south coast of the continent.

The high temperature variance in the northwest of the continent is just north of the maximum near-surface winds (arrows in Fig. 3a), and roughly collocated with the region of largest meridional temperature gradients (Fig. 3d). These large gradients reflect the relatively warm temperatures in the southwest of the continent, compared to the much colder southeast (Fig. 3b). Since temperatures are relatively uniform in the northern half of the continent, $\partial T/\partial y$ is larger on the west coast than on the east coast of the continent. The largest zonal temperature gradients are on the east and west coasts, at the boundaries between relatively warm ocean air and relatively cold continental air (Fig. 3c). That the maximum temperature variance is slightly west of the largest meridional temperature gradient, and more localized zonally, suggests that the enhanced zonal temperature gradients along the west coast contribute to the temperature variance maximum, though variations in τ_{eq}, τ_m, and EKE also play a role. We return to these in section 6.

The temperature pattern over the continent is set up in part by the mean flow advecting warm ocean air over the continent and in part by a strong, continental-scale anticyclone which is excited by the cold surface temperatures over the eastern part of the continent (Fig. 3e). Both act to warm the continent, compensating on a regional level for the strong cooling due to the land's small heat capacity. To quantify the relative contributions of the mean and stationary eddy flows to the temperature anomalies, we have decomposed the horizontal advection term in the stationary eddy temperature budget using Eq. (3). Figure 4a shows that mean flow advection is the largest contributor to the temperature pattern, warming the southern half of the continent, particularly the southwest. At higher latitudes the mean flow is weak and does not penetrate into the continental interior, which stays relatively cool. The anticyclone contributes to the temperature variance pattern by bringing relatively warm ocean air across the south coast of the continent, further warming the southwest, and then advecting this warm air toward the northeast of the continent, reducing the meridional temperature gradient in the east (Fig. 4b). The anticyclone also advects cold air to the southeast. Both the mean advection and

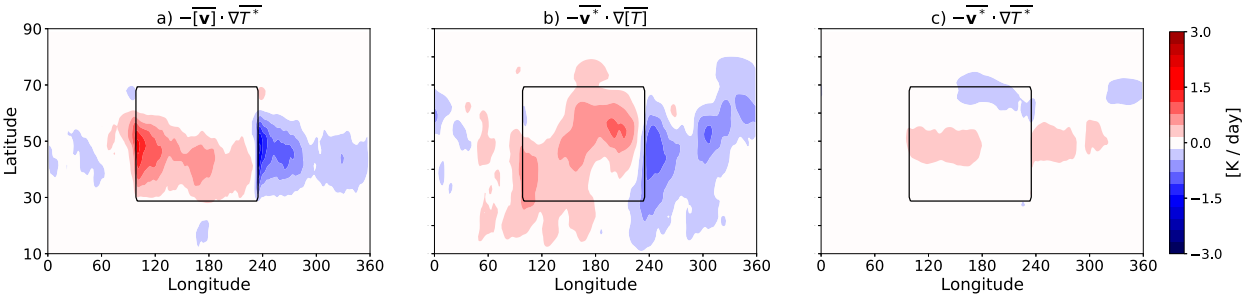

FIG. 4. (a) Contribution of the mean advection term in Eq. (3) to the winter 850-hPa zonal temperature anomalies in the Control experiment. (b) Contribution of the eddy advection term in Eq. (3) to the winter 850-hPa zonal temperature anomalies in the Control experiment. (c) Contribution of the nonlinear eddy advection term in Eq. (3) to the winter 850-hPa zonal temperature anomalies in the Control experiment.

the eddy advection terms cool the region off the continent's east coast by bringing relatively cold continental air over the western part of the ocean basin. The nonlinear eddy advection term is weak (Fig. 4c).

The importance of the zonal-mean wind for the temperature pattern suggests that the mean flow may be important for generating temperature variance. This would violate the framework underlying Eqs. (1) and (7), which assumes that temperature variance is primarily driven by transient eddies acting on mean temperature gradients. To assess the mean flow's contribution to the temperature variance, we have calculated the horizontal advection terms in the temperature variance budget [left-hand side of Eq. (4)]. Figure 5 confirms that transient eddies are the main factor determining regional temperature variance, as $\overline{\mathbf{v}'T'}\cdot\boldsymbol{\nabla}\overline{T}$ is by far the largest advective term (Fig. 5b). The mean flow contribution is weak, and mostly confined to the west coast of the continent (Fig. 5a), while the nonlinear contribution of transient eddies acting on temperature fluctuations damps temperature variance in the northwest somewhat (Fig. 5c). Hence, while the mean flow is essential for setting up the strong temperature gradients, it is not a major driver of temperature variance.

This Control case is the starting point for understanding the variance of wintertime temperatures over midlatitude continents and suggests that, in the absence of other geographic features (complex geometry, orography, etc.), a temperature variance maximum will be found in the northwest of a continent, just poleward of the maximum near surface winds. Variations in mean temperature are mostly due to mean flow advection, but the continental-scale anticyclone also contributes to the large temperature gradients in the western part of the continent. The variance itself is primarily due to transient eddies interacting with the seasonal-mean temperature gradients, and not due to the mean flow acting on temperature fluctuations.

4. The effects of continental geometry

a. *Varying continent size*

We now explore how the continent's climate is affected by changing its size and shape. We start by considering two cases which investigate continent size: a continent that is narrower in longitude and a continent that is longer in latitude (Figs. 2b,c).

The climate of the narrower continent, extending 60° in longitude rather than 135°, is similar to the Control case, except that the temperature anomalies over the continent are smaller (Fig. 6). The temperature gradients are correspondingly weaker, as is the temperature variance—the maximum daily variance in this case is 61 K^2 (Table 1, Fig. 6a). The smaller temperature anomalies are not surprising, as the narrower continent allows the mean flow to better smooth out the land–sea temperature contrast (Fig. 7a; note that the magnitude of this effect depends on the relative heat capacities of the land and ocean).

In the simulation with a long continent, extending to the equator (Fig. 2c), the anticyclone is stronger and centered farther south than in the Control case (Fig. 6j). The anticyclone also extends farther over the ocean to the northeast of the

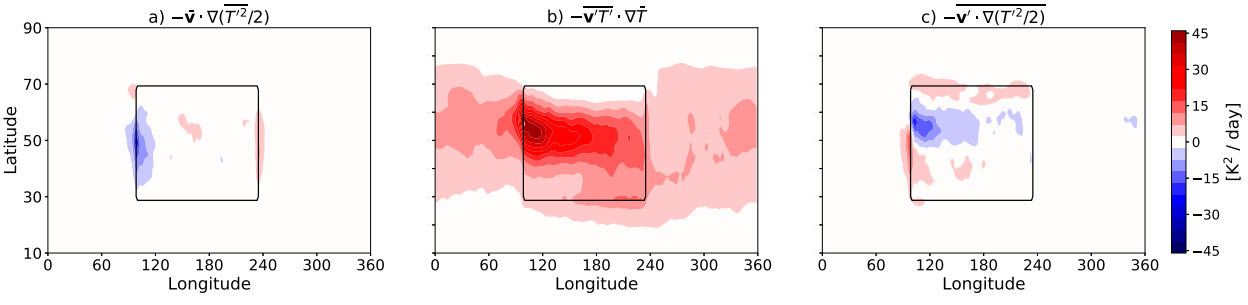

FIG. 5. Contributions of the three horizontal advection terms in Eq. (4) to the temperature variance budget in the Control simulation.

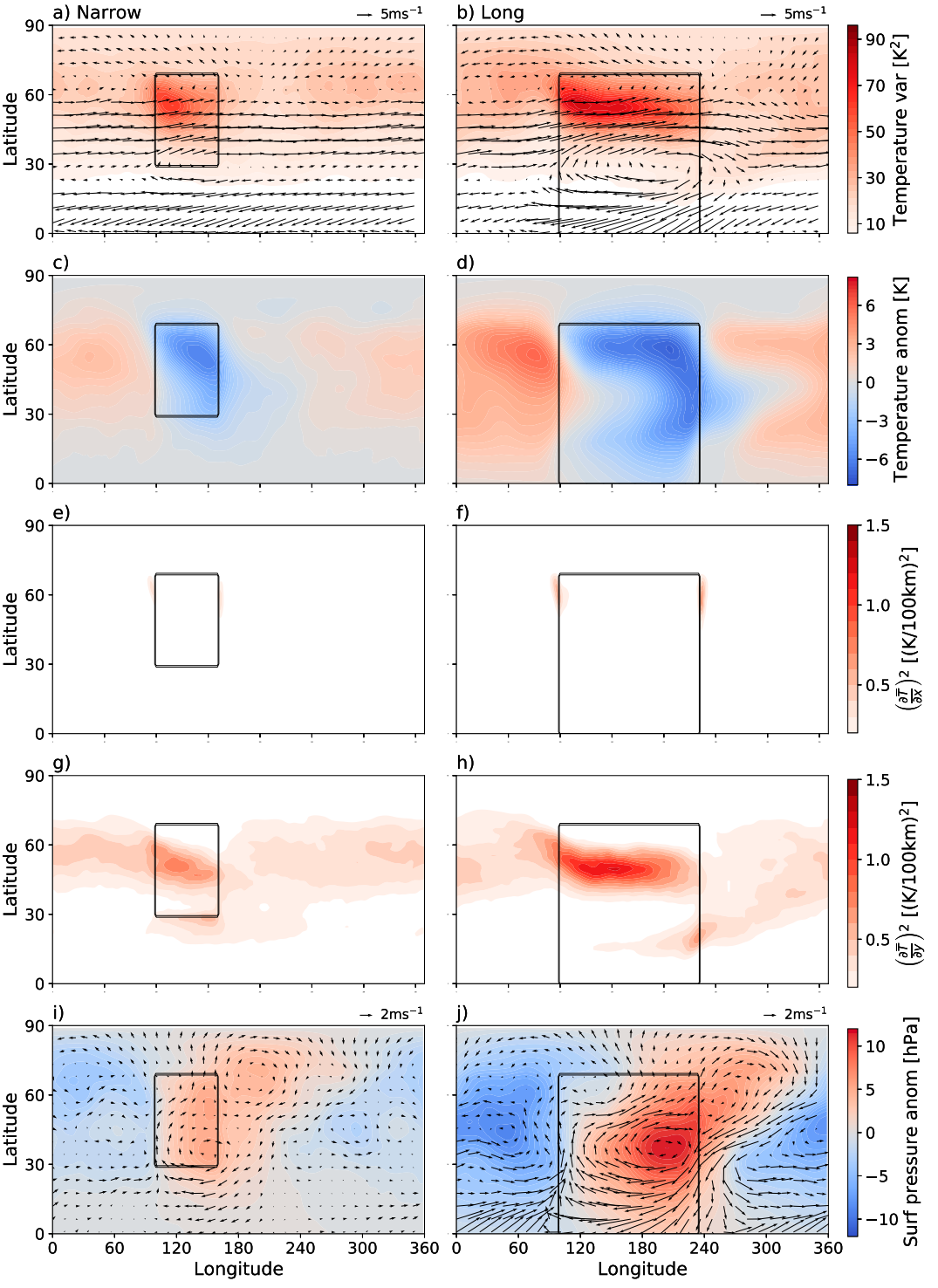

FIG. 6. (a) Variance of wintertime 850-hPa daily temperature in the Narrow simulation. (b) As in (a), but for the Long simulation. (c) Mean wintertime zonal 850-hPa temperature anomalies in the Narrow simulation. (d) As in (c), but for the Long simulation. (e) Mean wintertime squared zonal 850-hPa temperature gradients in the Narrow simulation. (f) As in (e), but for the Long simulation. (g) Mean wintertime squared meridional 850-hPa temperature gradients in the Narrow simulation. (h) As in (g,) but for the Long simulation. (i) Mean wintertime zonal surface pressure (colored contours) and 850-hPa wind anomalies (arrows) in the Narrow simulation. (j) As in (i), but for the Long simulation.

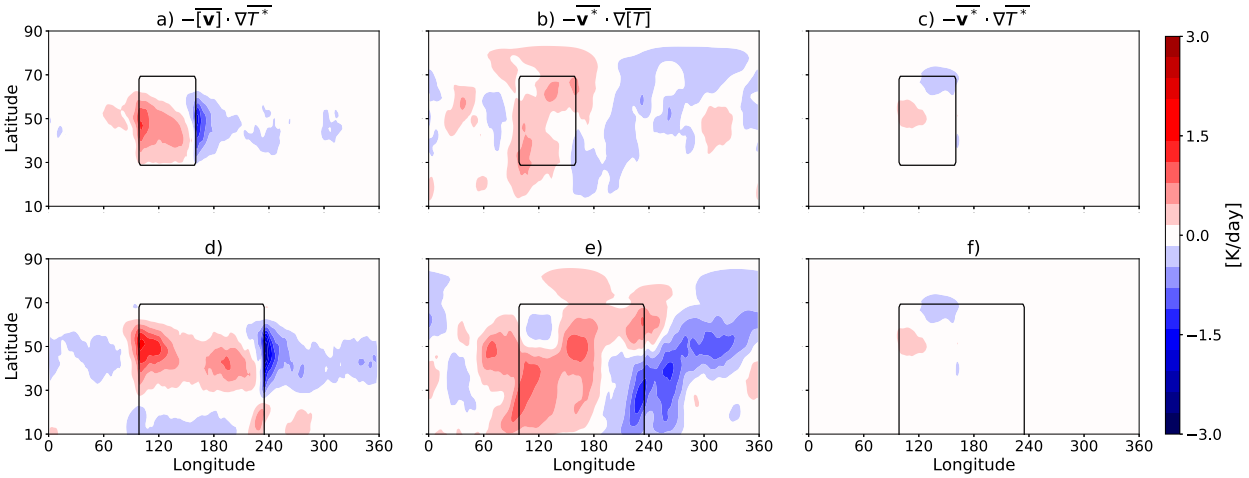

FIG. 7. (a) Contribution of the mean advection term in Eq. (3) to the winter 850-hPa zonal temperature anomalies in the Narrow experiment. (b) Contribution of the eddy advection term in Eq. (3) to the winter 850-hPa zonal temperature anomalies in the Narrow experiment. (c) Contribution of the nonlinear eddy advection term in Eq. (3) to the winter 850-hPa zonal temperature anomalies in the Narrow experiment. (d) As in (a), but for the Long experiment. (e) As in (b), but for the Long experiment. (f) As in (c), but for the Long experiment.

continent, while a cyclone sits over the rest of the midlatitude ocean. But the temperature gradients and variance over the continent are similar in midlatitudes, with a maximum daily temperature variance of 78 K^2, reflecting similar patterns of temperature advection (bottom row of Fig. 7). There is an additional region of enhanced temperature gradients in the southeast of the continent (Fig. 6h), though the gradients are weaker than in midlatitudes, and are maintained by the anticyclone, which brings cold northern air southward into the deep tropics (Fig. 7d). These large subtropical temperature gradients do not result in large temperature variances because eddy activity in the subtropics is weak (see section 6).

b. *Sloping coastlines*

The importance of mean-flow advection for shaping regional temperature distributions in the control simulation suggests that the shapes of the coastlines may be important for temperature variance. As mentioned above, Brayshaw et al. (2009) showed that the southwest–northeast slope of the North American east coast affects winter storm activity. We have run two experiments to explore this factor, motivated by the coastlines of North America and Eurasia. In the "Slanted" simulation (Fig. 2d), the east coast of the continent slants southwest to northeast, as it does for North America, while in the "Tapered" simulation the northwest border of the continent tapers so that the continent is shorter on its west coast than on its east coast (Fig. 2e). This mimics the tapering of Eurasia—the northern border of Eurasia is much farther south in western Europe than it is in central and east Asia.

In the Slanted experiment the maximum temperature gradients and variance are weaker than in the Control simulation (70 K^2, Fig. 8a), though the difference is not statistically significant. In many ways, the Slanted case is similar to the Control case, with an anticyclone centered over the east of the continent and relatively uniform temperatures in the north (Figs. 8c,i). The reason for the smaller variance is that the slanting coastline interferes with the anticyclone, weakening it and leading to smaller temperature gradients (because the eddy advection term in Eq. (3) is weaker; see Fig. 9b). The maximum surface pressure anomaly in this case is 9.7 hPa, compared to 11.0 hPa in the Control case, and the maximum meridional temperature gradient decreases from 1.17 to 1.04 K $(100\ km)^{-1}$.

The temperature variance is even weaker in the Tapered experiment, with a statistically significant decrease to a maximum of 65 K^2 (Fig. 8b). The winter climate of this case again retains many of the same basic features as the control experiment (Figs. 8d,j), but the southwest of the continent is now bordered by relatively warm ocean air to the north, reducing the strong temperature gradients which are seen in the northwest of the Control simulation (Fig. 8h). Instead, the largest temperature gradients are farther inland, and are relatively weak. Thus, cutting off the northwest corner of a continent substantially decreases the maximum temperature variance by eliminating the strong temperature gradients which would otherwise be present in the northwest.

c. *Bodies of water*

Finally, we present two experiments designed to investigate the role of bodies of water in shaping temperature distributions (Fig. 10). The "Gulf of Mexico" (GOM) case has a large bay in the southern coast of the continent (Fig. 2f), similar to the relatively warm Gulf of Mexico waters south of North America, and the "Inland Sea" case has a large inland body of water in the western part of the continent (Fig. 2g), mimicking the large bodies of water in western Eurasia: the Mediterranean, Black, and Caspian Seas.

The winter climates of both simulations are generally similar to the Control, though the maximum temperature variance is slightly higher in the GOM case (88 K^2) and lower in the Inland Sea case (78 K^2). The bodies of water do produce local

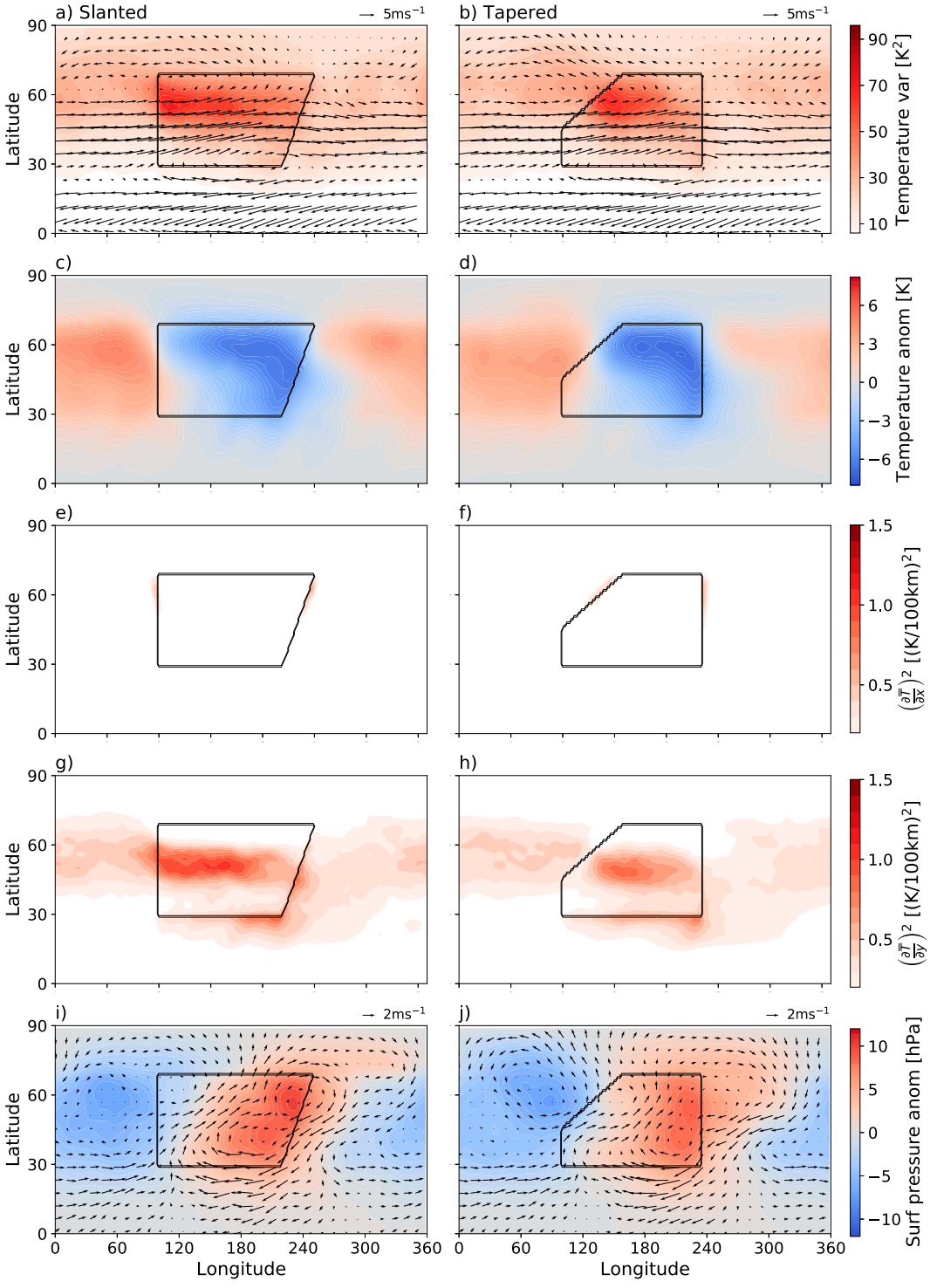

FIG. 8. As in Fig. 6, but for the (left) Slanted and (right) Tapered cases.

enhancements of temperature gradients and variance directly north of them (Figs. 10g,h), and in the Inland Sea case the maximum meridional temperature gradients are on the sea's north coast, but the highest temperature variance is still seen in the northwest of both continents. We return to this case in section 6.

While a large enough body of water would substantially alter the pattern of temperature variance over a continent, these simulations suggest that inland bodies of water are not a major factor in setting today's pattern of winter temperature variance.

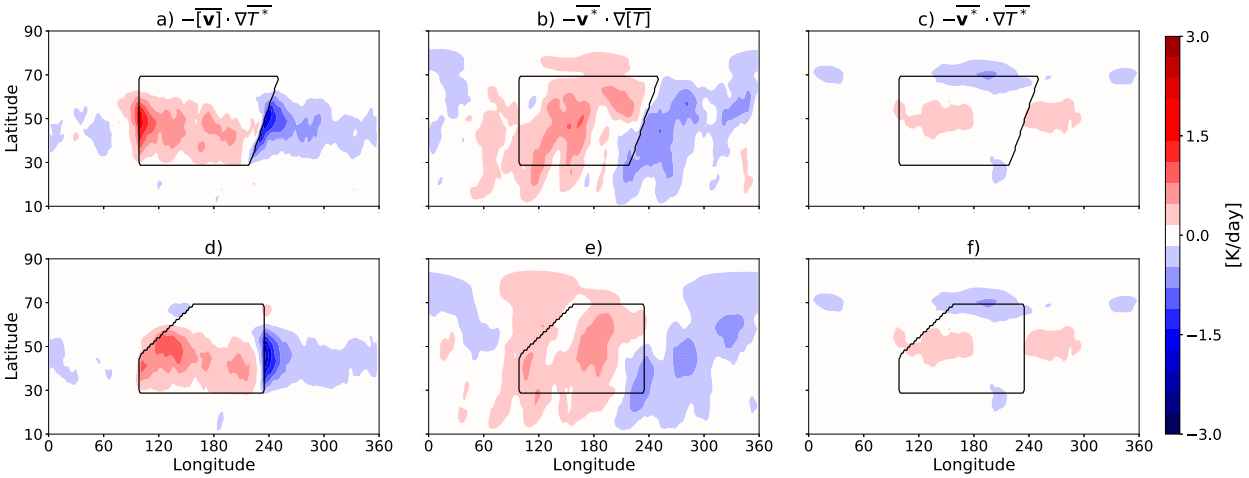

FIG. 9. As in Fig. 7, but for the (left) Slanted and (right) Tapered cases.

d. Comparing the simulations with observations

Comparing the results of this section with the observed pattern of temperature variance in Fig. 1 shows some similarities, but also important differences. The highest temperature variance over North America is located in the northwest part of the continent,[1] as seen in most of the experiments, while in Eurasia the highest variance is located north of the major orography in Central Asia (Tibet, the Himalayas, and the Mongolian mountains). In Lutsko et al. (2019), the maximum variance moved southward when the orography was flattened in GCM simulations, but stayed in Central Asia. This is consistent with the Tapered experiment in which the temperature variance is weak in "western Eurasia" because the tapering of the northern boundary of the continent eliminates the strong meridional temperature gradients which would otherwise be setup in the northwest of the continent. Orography further damps the variance over Eurasia.

The most notable inconsistency between our experiments and the observations is that according to the Narrow simulation the temperature variance should be weaker over the narrower North American continent than over the wider Eurasian continent—the reverse of what is observed. In fact, the Slanted experiment suggests that North America's sloping coastline may further damp temperature variance. So while the simulations presented above can explain the general patterns of temperature variance over the two continents, they cannot explain the relative magnitudes of the variance. To understand this better, in the next section we present experiments with two continents, which reveal how continental geometry interacts with stationary waves to determine regional temperature distributions.

5. Temperature variance over two continents

The addition of another continent generates stationary waves which impact temperature gradients and temperature variance, modifying the picture from the single-continent simulations. We first discuss a case with two midlatitude continents, of approximately the same widths as North America and Eurasia (80° and 120° in longitude, respectively; see Fig. 2h). In this case the narrower continent has substantially higher temperature variance than the wider continent (maximum of 77 K^2 compared to 69 K^2, Table 1, Fig. 11a), as well as stronger temperature gradients (Figs. 11e,g), resembling what is observed in Earth's Northern Hemisphere much more than the Narrow simulation presented in section 4a. Examining the temperature anomalies and flow fields shows that the combined presence of the two continents leads to weaker surface pressure anomalies compared to a single continent (Fig. 11i), because the greater land area in this case cools the entire Northern Hemisphere (not shown), and leads to weaker anticyclones compared to the single continent cases. The narrower "North American" continent does not produce a significant stationary wave response away from the continent, while the surface pressure anomaly over the larger "Eurasian" continent is strong enough to excite a stationary wave that extends over the "Pacific," with a cyclone off the west coast of the narrower continent and anomalously warm temperatures in the "east Pacific." The cyclone interacts with the anticyclone over the eastern part of the narrower continent to produce strong southwesterly flow over the narrow continent, while the warm temperatures off the narrower continent's west coast also lead to enhanced mean flow temperature advection (top row of Fig. 12). Together, these produce large temperature gradients over the narrow continent. By contrast, the weaker stationary wave generated by the narrow continent leads to weaker eddy temperature advection and to weaker mean flow advection, which acts on relatively cold temperatures over the "Atlantic."

While the 2 Continent case produces a substantial difference in the temperature variance of the continents that is qualitatively consistent with the observations, we noted in the previous section that the climate of the Tapered simulation was similar in some respects to that of Eurasia, and that Eurasia's tapered northwest coast could partly explain why temperature variance is so low over the continent. As such, we present a final simulation

[1] The highest variance is in the lee of the Rockies, but still in the northwest quadrant of the continent.

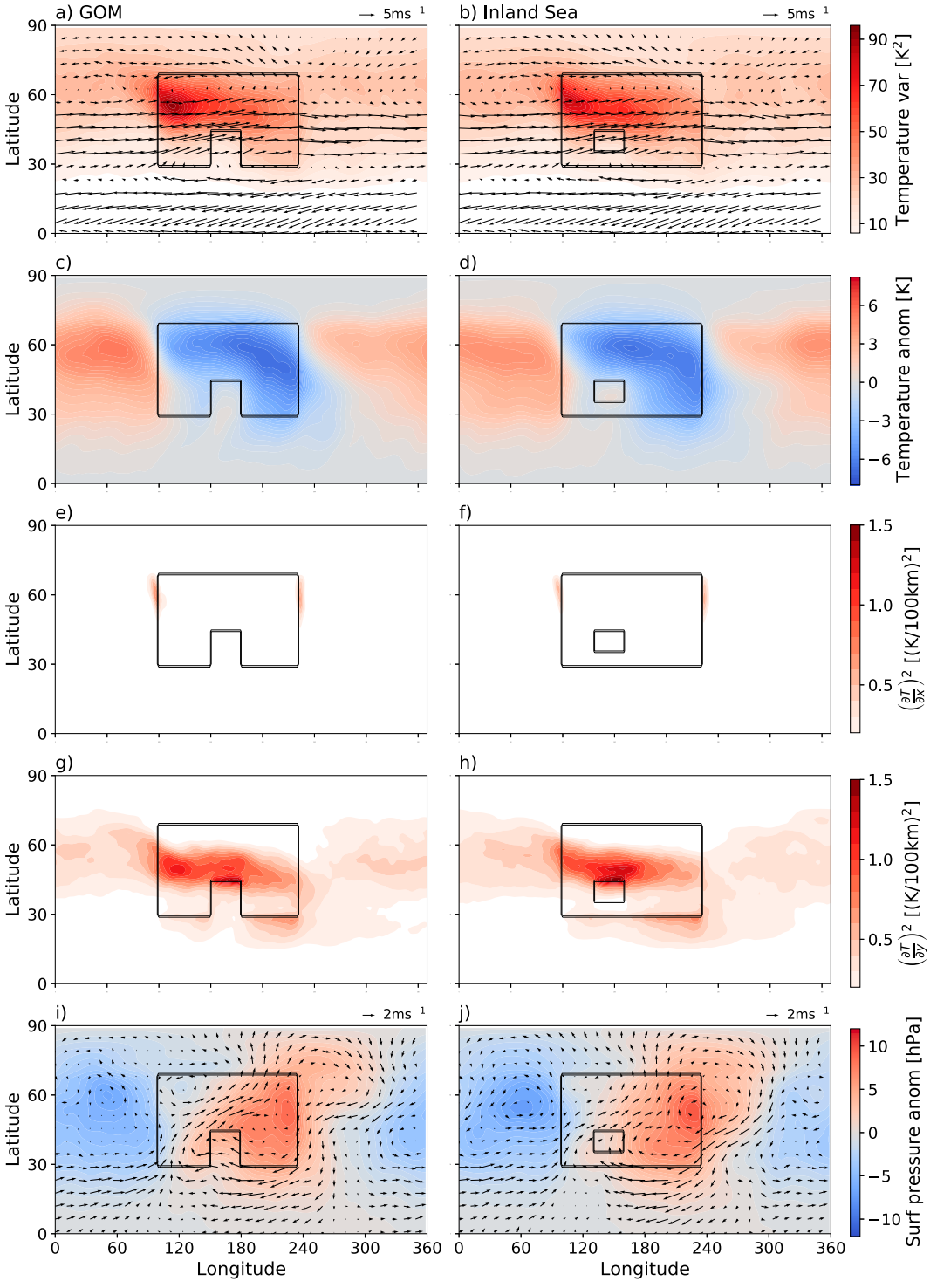

FIG. 10. As in Fig. 6, but for the (left) GOM and (right) Inland Sea cases.

in which the north coast of the wider continent is tapered, similar to the tapering of Eurasia's northwest coast (Fig. 2i).

Tapering weakens the difference in temperature variance between the two continents, with the maximum over the narrower continent decreasing to 65 K^2 and over the wider continent to 61 K^2. The reason for this is that the tapering weakens the stationary wave over the wider continent, and, hence, also the southwesterly flow over the narrow continent

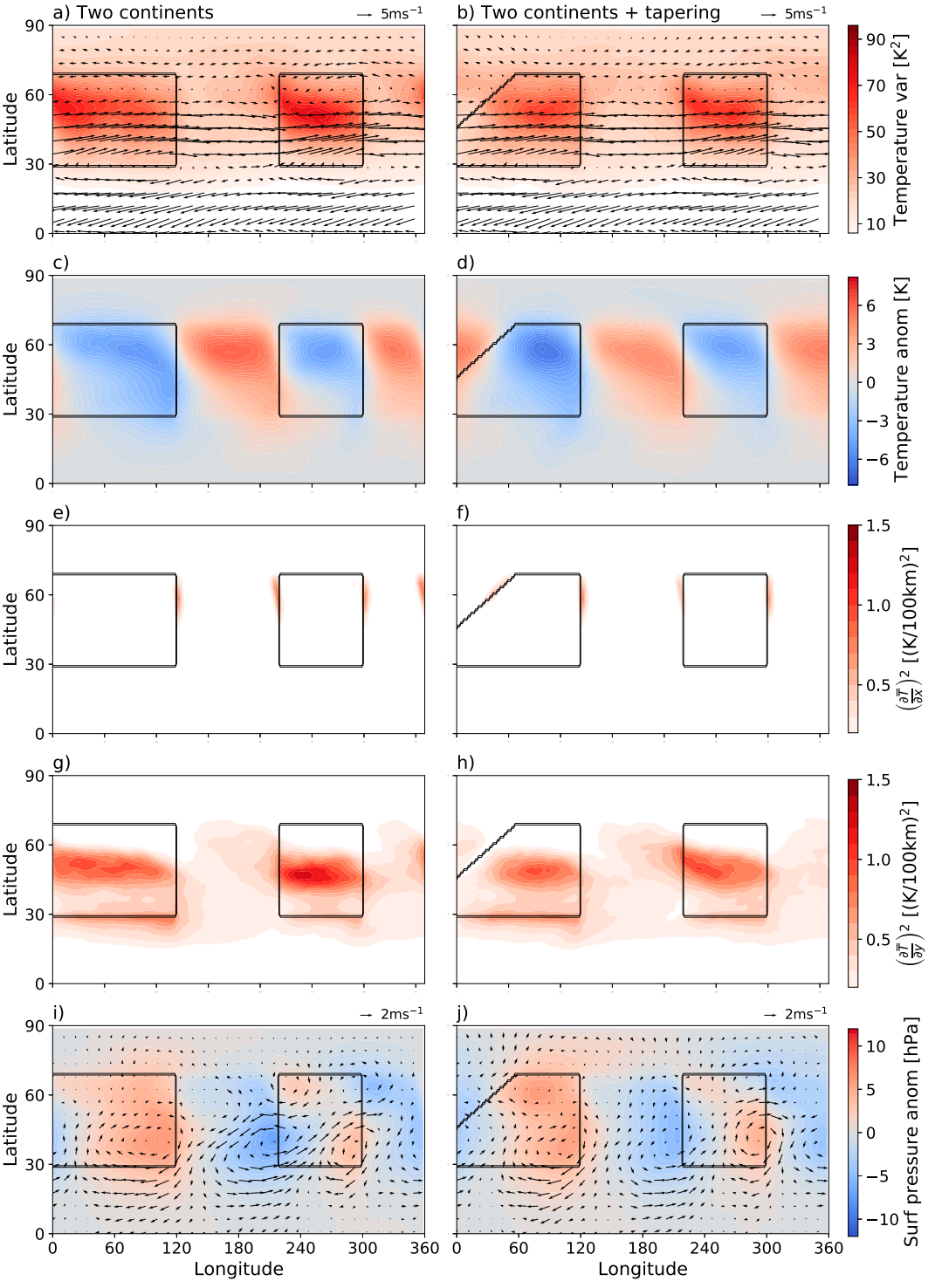

FIG. 11. As in Fig. 6, but for (left) the simulation with two continents and (right) the simulation with two continents and tapering.

(Figs. 11d,j). The zonal temperature anomalies over the "east Pacific" are smaller, so the zonal temperature anomalies advected by the mean flow are cooler, and the mean flow advection is weaker (cf. Figs. 12d and 12a). The eddy temperature advection is also weaker. Thus, the tapering of the wider continent produces smaller temperature gradients over the narrower continent, and weaker temperature variance.

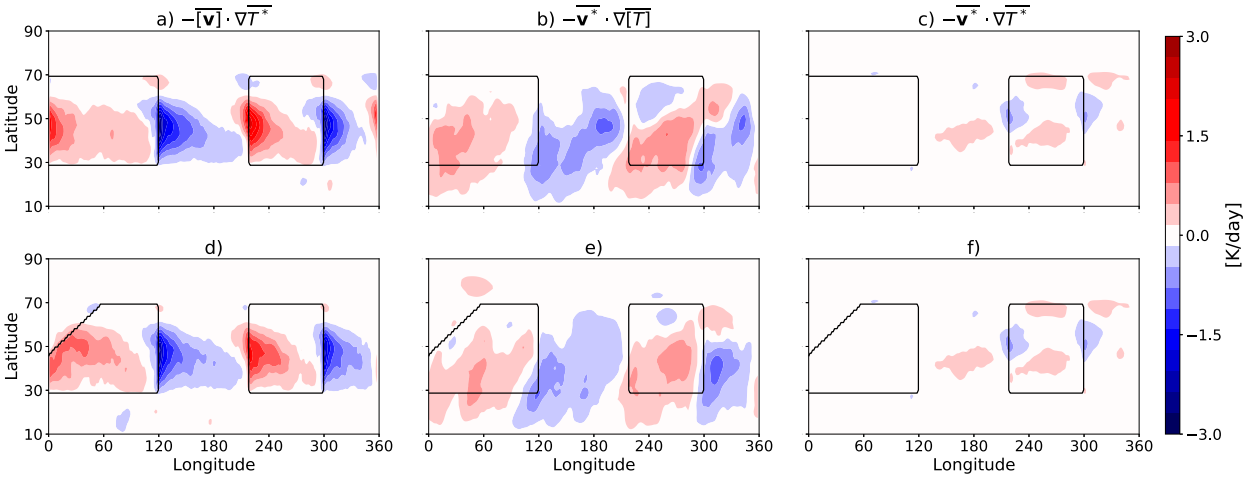

FIG. 12. As in Fig. 7, but for (top) the simulation with two continents and (bottom) the simulation with two continents and tapering.

Nevertheless, we believe this case is instructive for understanding the observed pattern of temperature variance. The stationary wave patterns in Figs. 11c and 11d are very different from the observed Northern Hemisphere winter stationary wave pattern, as important wave sources, such as Asian orography and diabatic heating over the west Pacific are missing from the simulations. These would alter the simulated stationary wave field, and would mostly affect temperatures over North America rather than over Eurasia. Hence, the relatively low temperature variance over Eurasia can be thought of as a primarily local effect, caused by the tapering of the northwest coast of Europe, whereas the enhanced temperature variance over North America is a nonlocal effect, driven by a stationary wave pattern that produces enhanced temperature gradients over North America.

6. Effective mixing lengths and eddy kinetic energy

The above discussion has primarily focused on temperature gradients as driving regional differences in temperature variance, as these have previously been identified as the primary control on midlatitude temperature variance (e.g., Schneider et al. 2015). We confirm that this is the case here in Fig. 13, which plots the maximum temperature variance against the maximum squared meridional temperature gradients across the simulations (circular markers). The points generally cluster around a straight line ($r^2 = 0.77$), though there are some hints of nonlinearity for the two cases with the largest variance (the Control and GOM cases). Similar results are obtained by plotting the maximum temperature variance against the maximum value of $(\partial T/\partial y)^2 + (\partial T/\partial x)^2$ (crosses in same figure, $r^2 = 0.71$), and the slopes give effective mixing lengths of 677 and 658 km, respectively. Hence, variations in temperature gradients are the main driver of variations in temperature variance across the simulations.

More evidence for the importance of temperature gradients comes from the left panels of Fig. 14, which show the eddy kinetic energy (Fig. 14a) and the squared temperature gradients $[(\partial T/\partial y)^2 + (\partial T/\partial x)^2$, Fig. 14c] in the Control simulation. In the Control simulation, the EKE is largest at midlatitudes, between roughly 40° and 60°N, and is maximal over the continent. This is consistent with the large temperature gradients over the continent, which drive stronger eddy activity (e.g., through larger Eady growth rates). While there is an EKE maximum roughly collocated with the maximum temperature variance, the EKE is high throughout the continent, and there are maxima with similar magnitudes in the eastern part of the continent. So the EKE alone cannot explain the strong temperature variance in the northwest. The EKE map can explain why extending the length of the continent to lower latitudes does not produce large subtropical temperature variance maxima (section 4a), as the values are very small south of about 30°N.

The squared temperature gradients resemble the temperature variance much more closely (Fig. 14c), particularly the strong east–west gradient. This confirms again that to first

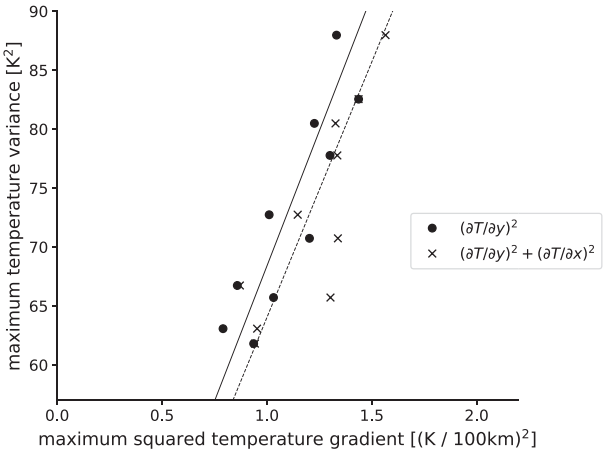

FIG. 13. Maximum 850-hPa temperature variance vs maximum squared temperature gradients [either $(\partial T/\partial y)^2$ (round markers) or $(\partial T/\partial y)^2 + (\partial T/\partial x)^2$ (crosses)] for the various simulations. Separate values are plotted for each continent in the 2 continent simulations. The lines show fits to the data using reduced major axis regression.

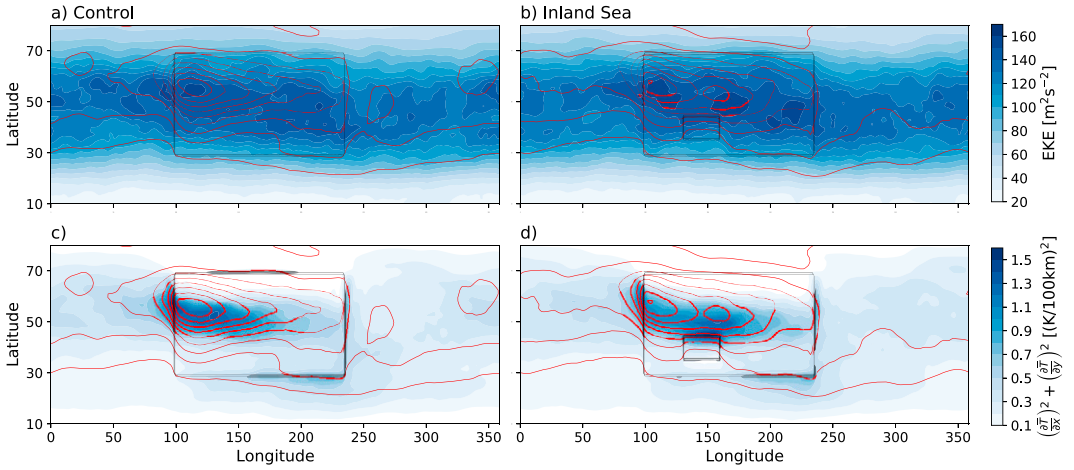

FIG. 14. (a) Wintertime 850-hPa eddy kinetic energy (blue shading) and daily temperature variance (red contours, contour interval = 9 K^2) in the Control simulation. (b) As in (a), but for the Inland Sea simulation. (c) Wintertime near-surface 850-hPa squared temperature gradients $[(\partial T/\partial y)^2 + (\partial T/\partial x)^2]$ (blue shading) and daily temperature variance (red contours, same contour interval) in the Control simulation. (d) As in (c), but for the Inland Sea simulation.

order temperature gradients govern the pattern of temperature variance in these simulations. The two time scales identified in section 2b (τ_{eq} and τ_m) could also play roles in setting the spatial patterns of temperature variance, but estimating them is beyond the scope of this study. We note that the land–sea difference in heat capacity likely causes τ_{eq} to be larger over the continents, and in section 2b it was argued that τ_m should be related to surface friction or surface roughness, which is constant throughout the domain. So we expect that τ_{eq} contributes to the temperature variance pattern, but not τ_m.

The panels on the right of Fig. 14 show the EKE and squared temperature gradients for the Inland Sea simulation, which is the case in which EKE variations seem to play the largest role in determining regional temperature variance. There are large temperature gradients in the northwest of the continent and also to the northwest of the inland sea. In fact, the largest temperature gradients are on the sea's north coast. Both of these regions of strong temperature gradients produce temperature variance maxima, but the strongest variance is in the northwest of the continent. This seems to be because the EKE is slightly larger there, though variations in τ_m or τ_{eq} could also play roles in keeping the maximum temperature variance in the northwest of the continent.

7. Conclusions

In this study, we have investigated how continental geometry affects near-surface temperature variance over midlatitude continents. We began by discussing a Control simulation, which shows that in the case of an isolated, rectangular midlatitude continent, temperature variance maxima are found in the northwest of continents, poleward of the maximum near surface winds and collocated with the maximum horizontal temperature gradients. These strong temperature gradients are mostly due to mean-flow advection, but a continental-scale winter anticyclone also contributes to the high temperature variance in the northwest. To our knowledge, this case has not been discussed before, and is a starting point for what temperature variance should look like over midlatitude continents.

Building on the Control experiment, we have run a variety of cases designed to mimic key aspects of the geographies of North America and Eurasia. These simulations have provided several insights into how continental geometry shapes regional temperature variance:

- In isolation, narrower continents have weaker temperature variance maxima, because mean flow advection smooths out land–sea temperature contrasts. By contrast, the length of a continent in latitude does not affect temperature variance at midlatitudes, though it can produce weak temperature variance maxima in the subtropics. Subtropical temperature variance is generally weak because of the low EKE there.
- The shapes of the eastern and western coastlines are important factors governing temperature variance. A sloping east coast weakens the continental anticyclone, which advects less warm air over the southwest of the continent, reducing the maximum temperature gradients and temperature variance. The west coast has an even stronger effect, as a tapered northwestern coast (similar to the tapering of Eurasia) eliminates the strong temperature gradients in the northwest of the continent, greatly damping temperature variance.
- Inland bodies of water, like the Gulf of Mexico, and inland seas, like the Mediterranean, Black and Caspian Seas, can lead to local maxima in temperature variance, but for the cases we considered the maximum temperature variance is still in the northwest of the continent, and is relatively insensitive to bodies of water.

While these simulations can explain some of the features of observed temperature distributions, there is a key discrepancy: the Narrow simulation suggests that temperature variance should be weaker over North America than over Eurasia, not

larger. To resolve this difference, we have run simulations with two continents: one wider and one narrower, mimicking Eurasia and North America, respectively. In this case, the temperature variance is larger over the narrower continent, because the stationary wave excited by the wider continent warms the "Pacific," enhancing mean flow advection of heat over the narrow continent and strengthening its temperature gradients. We have attempted to add an extra degree of realism to this configuration by tapering the northwest coast of the wider continent, similar to the tapering of western Eurasia. The tapering reduces the temperature variance over the wider continent, but also weakens the stationary wave excited by the continent, weakening the temperature gradients and variance over the narrower continent.

Together, these results suggest that the tapering of northwestern Eurasia plays a key role in damping temperature variance over the continent. Combined with the findings of Lutsko et al. (2019), the weak wintertime temperature variance over Eurasia can be largely explained by the local effects of a tapered northwest coast and the presence of large mountain ranges in central and east Asia (Tibet, the Himalayas, and the Mongolian mountains), which damp upstream temperature variance. Conversely, the high temperature variance over North America must be due to nonlocal effects (i.e., stationary waves); on its own, a narrow continent would be expected to have low temperature variance. Explaining the high temperature variance over North America thus requires a full picture of the wintertime stationary wave pattern over the Pacific. Garfinkel et al. (2020) recently showed that the observed stationary wave pattern is a nonlinear combination of land–sea contrasts, horizontal heat fluxes in the ocean and topography. In fact, over the northeast Pacific and western North America, the sum of the responses to each forcing is opposite to that when all three are imposed simultaneously due to nonlinear interactions among the forcings. So it would be difficult to reproduce the high variance over North America without including all of the major wave sources in east Asia, the west Pacific, and North America.

Changes in effective mixing lengths appear to play a small role in determining the differences in variance between the various simulations, though explaining the regional structure of the time scales in Eq. (7) is difficult, and left for future work. Brayshaw et al. (2009) noted that increased surface roughness over land reduces EKE, and in our framework would also lead to a smaller τ_m. The lack of surface roughness differences and of a realistic land model are important limitations to the present work.

As a final note, although our primary motivation has been explaining the present-day pattern of temperature variance, our results may also be helpful for interpreting the patterns of temperature variance in past climates, when Earth's continents had very different geographies. In particular, the single-continent simulations may provide a starting point for studying continental temperature distributions during periods when Earth's surface featured a supercontinent, such as Pangaea (336–175 Mya) and Gondwana (550–336 Mya) (Palin and Santosh 2021).

Acknowledgments. This work was much improved by helpful feedback from Editor Isla Simpson and three anonymous reviewers. We thank Daniel Koll and Clair Nichols for helpful discussions and feedback on an earlier version of this manuscript. N.K.N and N.J.L. were supported by NSF Grant OCE-2023483.

Data availability statement. Analysis scripts and sample namelist files are available at https://github.com/nicklutsko/Temperature_Variance_Continental_Geometry/.

REFERENCES

Barnes, E. A., and L. M. Polvani, 2015: CMIP5 projections of Arctic amplification, of the North American/North Atlantic circulation, and of their relationship. *J. Climate*, **28**, 5254–5271, https://doi.org/10.1175/JCLI-D-14-00589.1.

Blackport, R., J. A. Screen, K. van der Wiel, and R. Bintanja, 2019: Minimal influence of reduced Arctic sea ice on coincident cold winters in mid-latitudes. *Nat. Climate Change*, **9**, 697–704, https://doi.org/10.1038/s41558-019-0551-4.

Brayshaw, D. J., B. Hoskins, and M. Blackburn, 2009: The basic ingredients of the North Atlantic storm track. Part I: Land–sea contrast and orography. *J. Atmos. Sci.*, **66**, 2539–2558, https://doi.org/10.1175/2009JAS3078.1.

Caballero, R., and J. Hanley, 2012: Midlatitude eddies, storm-track diffusivity, and poleward moisture transport in warm climates. *J. Atmos. Sci.*, **69**, 3237–3250, https://doi.org/10.1175/JAS-D-12-035.1.

Cohen, J., and Coauthors, 2014: Recent Arctic amplification and extreme mid-latitude weather. *Nat. Geosci.*, **7**, 627–637, https://doi.org/10.1038/ngeo2234.

Ferrari, R., and M. Nikurashin, 2010: Suppression of eddy diffusivity across jets in the Southern Ocean. *J. Phys. Oceanogr.*, **40**, 1501–1519, https://doi.org/10.1175/2010JPO4278.1.

Fischer, E. M., and C. Schär, 2009: Future changes in daily summer temperature variability: Driving processes and role for temperature extremes. *Climate Dyn.*, **33**, 917, https://doi.org/10.1007/s00382-008-0473-8.

Frierson, D. M. W., 2007: The dynamics of idealized convection schemes and their effect on the zonally averaged tropical circulation. *J. Atmos. Sci.*, **64**, 1959–1976, https://doi.org/10.1175/JAS3935.1.

——, I. M. Held, and P. Zurita-Gotor, 2006: A gray-radiation aquaplanet moist GCM. Part I: Static stability and eddy scales. *J. Atmos. Sci.*, **63**, 2548–2566, https://doi.org/10.1175/JAS3753.1.

Garfinkel, C. I., and N. Harnik, 2017: The non-Gaussianity and spatial asymmetry of temperature extremes relative to the storm track: The role of horizontal advection. *J. Climate*, **30**, 445–464, https://doi.org/10.1175/JCLI-D-15-0806.1.

——, I. White, E. P. Gerber, M. Jucker, and M. Erez, 2020: The building blocks of Northern Hemisphere wintertime stationary waves. *J. Climate*, **33**, 5611–5633, https://doi.org/10.1175/JCLI-D-19-0181.1.

Held, I. M., R. L. Panetta, and R. T. Pierrehumbert, 1985: Stationary external Rossby waves in vertical shear. *J. Atmos. Sci.*, **42**, 865–883, https://doi.org/10.1175/1520-0469(1985)042<0865:SERWIV>2.0.CO;2.

——, M. Ting, and H. Wang, 2002: Northern winter stationary waves: Theory and modeling. *J. Climate*, **15**, 2125–2144,

https://doi.org/10.1175/1520-0442(2002)015<2125:NWSWTA>2.0.CO;2.

Holmes, C. R., T. Woollings, E. Hawkins, and H. de Vries, 2016: Robust future changes in temperature variability under greenhouse gas forcing and the relationship with thermal advection. *J. Climate*, **29**, 2221–2236, https://doi.org/10.1175/JCLI-D-14-00735.1.

Hoskins, B., and T. Woollings, 2015: Persistent extratropical regimes and climate extremes. *Curr. Climate Change Rep.*, **1**, 115–124, https://doi.org/10.1007/s40641-015-0020-8.

Kushner, P. J., and I. M. Held, 1998: A test, using atmospheric data, of a method for estimating ocean eddy diffusivity. *Geophys. Res. Lett.*, **25**, 4213–4216, https://doi.org/10.1029/1998GL900142.

Linz, M., G. Chen, and Z. Hu, 2018: Large-scale atmospheric control on non-Gaussian tails of midlatitude temperature distributions. *Geophys. Res. Lett.*, **45**, 9141–9149, https://doi.org/10.1029/2018GL079324.

——, ——, B. Zhang, and P. Zhang, 2020: A framework for understanding how dynamics shape temperature distributions. *Geophys. Res. Lett.*, **47**, e2019GL085684, https://doi.org/10.1029/2019GL085684.

Lutsko, N. J., J. W. Baldwin, and T. W. Cronin, 2019: The impact of large-scale orography on Northern Hemisphere winter synoptic temperature variability. *J. Climate*, **32**, 5799–5814, https://doi.org/10.1175/JCLI-D-19-0129.1.

McKinnon, K. A., A. R. Stine, and P. Huybers, 2013: The spatial structure of the annual cycle in surface temperature: Amplitude, phase, and Lagrangian history. *J. Climate*, **26**, 7852–7862, https://doi.org/10.1175/JCLI-D-13-00021.1.

O'Gorman, P. A., and T. Schneider, 2008: The hydrological cycle over a wide range of climates simulated with an idealized GCM. *J. Climate*, **21**, 3815–3832, https://doi.org/10.1175/2007JCLI2065.1.

Palin, R. M., and M. Santosh, 2021: Plate tectonics: What, where, why, and when? *Gondwana Res.*, **100**, 3–24, https://doi.org/10.1016/j.gr.2020.11.001.

Schneider, T., T. Bischoff, and H. Plotka, 2015: Physics of changes in synoptic midlatitude temperature variability. *J. Climate*, **28**, 2312–2331, https://doi.org/10.1175/JCLI-D-14-00632.1.

Screen, J. A., 2014: Arctic amplification decreases temperature variance in northern mid- to high-latitudes. *Nat. Climate Change*, **4**, 577–582, https://doi.org/10.1038/nclimate2268.

——, and R. Blackport, 2019: How robust is the atmospheric response to projected Arctic sea ice loss across climate models? *Geophys. Res. Lett.*, **46**, 11 406–11 415, https://doi.org/10.1029/2019GL084936.

——, and Coauthors, 2018: Consistency and discrepancy in the atmospheric response to Arctic sea-ice loss across climate models. *Nat. Geosci.*, **11**, 155–163, https://doi.org/10.1038/s41561-018-0059-y.

Simpson, I. R., and Coauthors, 2020: An evaluation of the large-scale atmospheric circulation and its variability in CESM2 and other CMIP models. *J. Geophys. Res. Atmos.*, **125**, e2020JD032835, https://doi.org/10.1029/2020JD032835.

Tamarin-Brodsky, T., K. Hodges, B. J. Hoskins, and T. G. Shepherd, 2019: A dynamical perspective on atmospheric temperature variability and its response to climate change. *J. Climate*, **32**, 1707–1724, https://doi.org/10.1175/JCLI-D-18-0462.1.

——, ——, ——, and ——, 2020: Changes in Northern Hemisphere temperature variability shaped by regional warming patterns. *Nat. Geosci.*, **13**, 414–421, https://doi.org/10.1038/s41561-020-0576-3.

Vargas Zeppetello, L. R., and D. S. Battisti, 2020: Projected increases in monthly midlatitude summertime temperature variance over land are driven by local thermodynamics. *Geophys. Res. Lett.*, **47**, e2020GL090197, https://doi.org/10.1029/2020GL090197.

Zhang, B., M. Linz, and G. Chen, 2022: Interpreting observed temperature probability distributions using a relationship between temperature and temperature advection. *J. Climate*, **35**, 705–724, https://doi.org/10.1175/JCLI-D-20-0920.1.